A Fracture Criterion for the Notch Strength of High Strength Steels in the Presence of Hydrogen

C. Ayas[a], V.S. Deshpande[a], N.A Fleck[a,*]

[a]*Department of Engineering, Cambridge University, Trumpington Street, Cambridge CB2 1PZ, UK*

Abstract

High strength steels can suffer from a loss of ductility when exposed to hydrogen, and this may lead to sudden failure. The hydrogen is either accommodated in the lattice or is trapped at defects, such as dislocations, grain boundaries and carbides. The challenge is to identify the effect of hydrogen located at different sites upon the drop in tensile strength of a high strength steel. For this purpose, literature data on the failure stress of notched and un-notched steel bars are re-analysed; the bars were tested over a wide range of strain rates and hydrogen concentrations. The local stress state at failure has been determined by the finite element (FE) method, and the concentration of both lattice and trapped hydrogen is predicted using Oriani's theory along with the stress-driven diffusion equation. The experimental data are rationalised in terms of a postulated failure locus of peak maximum principal stress versus lattice hydrogen concentration. This failure locus is treated as a unique material property for the given steel and heat treatment condition. We conclude that the presence of lattice hydrogen increases the susceptibility to hydrogen embrittlement whereas trapped hydrogen has only a negligible

*Corresponding author *E-mail address:* naf1@eng.cam.ac.uk

effect. It is also found that the observed failure strength of hydrogen-charged un-notched bars is less than the peak local stress within the notched geometries. Weakest link statistics are used to account for this stressed volume effect.
Keywords: Hydrogen embrittlement, Hydrogen trapping, Weakest link statistics.

1. Introduction

Steels, when exposed to hydrogen, suffer from a loss of ductility and toughness and this may lead to sudden, premature failure. Consequently, the adverse effects of hydrogen embrittlement must be included in engineering design for applications such as pipelines and nuclear power plants that come into contact with water, hydrocarbons or hydrogen gas. Hydrogen embrittlement is also critical for welded joints since hydrogen take-up can arise from the use of damp electrodes in electric welding operations.

The atomistic mechanism of hydrogen embrittlement remains a controversial issue: at least two major mechanisms have been proposed. According to the Hydrogen Induced Decohesion (HID) mechanism, hydrogen which has accumulated at a crack tip reduces the cohesive strength giving rise to a reduced fracture toughness (Troiano, 1960; Oriani, 1972). In contrast, the Hydrogen Enhanced Localized Plasticity (HELP) mechanism (see for example Birnbaum and Sofronis (1994)), assumes that hydrogen redistribution occurs around dislocations, reduces the elastic interaction energy between dislocations and thereby decreases the Peierls stress. Material softening then ensues.

Gangloff (2003) argued that HID is the dominant mechanism in high strength alloys on the basis that a wide range of micromechanical fracture toughness models of HID are able to predict (i) the threshold stress intensity factor K_{ISCC} and (ii) the crack growth rate da/dt versus K response for hydrogen exposed alloys; see, for example, Gerberich et al. (1991) for a model based on crack tip dislocation mechanics. Serebrinsky et al. (2004) support Gangloff's (2003) view by developing a quantitative HID based model: they assumed that a cohesive zone exists at a crack tip and the strength of the cohesive zone drops with increasing local hydrogen concentration. By suitable adjustment of material parameters, this model was able to predict the observed incubation time for crack initiation, the effect of hydrogen concentration upon K_{ISCC} and the effect of temperature upon da/dt. The HID mechanism is also supported by first principles calculations; see for example Jiang and Carter (2004) who demonstrated that the surface energy decreases sharply with increasing hydrogen concentration. Recently, Novak et al. (2010) proposed a synergetic effect of the HID and HELP mechanisms. They argued that the HELP mechanism reduces the length of pile-ups on carbides situated at the grain boundaries. Simultaneously, the presence of hydrogen reduces the cohesive toughness of the grain boundaries (HID), giving rise to premature inter-granular fracture.

Loading rate also plays an important role upon the fracture mode and the threshold stress intensity factor K_{ISCC} of high strength alloys exposed to hydrogen (Gangloff, 2003). Thomas et al. (2003) measured K_{ISCC} in ultra high strength steel specimens charged with hydrogen, and found that $K_{ISCC} \approx 0.1 K_{IC}$ when the loading rate was below $dK/dt = 0.3$ MPa$\sqrt{\text{m}}$/s,

where K_{IC} is the fracture toughness measured in the absence of hydrogen. In contrast, for loading rates greater than $dK/dt = 0.7$ MPa$\sqrt{\text{m}}$/s, the threshold stress intensity factor was found to be $K_{ISCC} \approx 0.4K_{IC}$. Associated with this increase in K_{ISCC} is a change in fracture mode from cleavage to micro-void coalescence; see Thomas et al. (2003).

The effect of hydrogen *trapping* at microstructural defects upon hydrogen embrittlement remains a controversial issue, see Gangloff (2003). It is unclear whether embrittlement is due to trapped hydrogen (for example at carbide particles and at dislocations) or is mainly due to lattice hydrogen. Li et al. (2004) argued that trapping sites such as martensite interfaces, austenite grain boundaries, and dislocation cores possessing a strong affinity to hydrogen can prevent hydrogen from segregating to crack tip and mitigate against hydrogen embrittlement. Yamasaki and Bhadeshia (2006) shares this view and investigated the peak trapping affinity of carbides to hydrogen in martensitic steels in order to mitigate the detrimental effects of hydrogen upon mechanical performance. In contrast, Novak et al. (2010) conjectured that hydrogen trapped at the dislocations is the dominant source of embrittlement in high strength steels.

In this paper, we shall analyse the sensitivity of the tensile strength of a high strength steel to the presence of hydrogen at lattice interstitial sites and trapped at defects. To achieve this, the experimental data of Wang et al. (2005b, 2007) and Hagihara et al. (2008) are analysed for AISI 4135 steel. Both sets of authors considered notched bars and measured the tensile strength for a wide range of hydrogen charging conditions, and for selected values of notch radius. We shall show below that the test times

employed by the Wang et al. (2005b) are sufficiently large for hydrogen diffusion to attain equilibrium. In contrast Hagihara et al. (2008) performed rapid tests in relation to the diffusion time for hydrogen.

It is notoriously difficult to measure accurately the amount of absorbed hydrogen and its relative partitioning between various sites in a steel microstructure. Here, we will calculate the trapped and lattice hydrogen concentrations using Oriani's theory, and the stress-driven diffusion equation; the procedure will be explained in some detail in Section 2. Since this analysis requires a knowledge of the stress and strain state of the solid, an elastic-plastic FE model is used in order to obtain these field quantities.

Sofronis and McMeeking (1989) gave the governing field equations for hydrogen diffusion in a plastically deforming solid. They assumed that the relative concentration of hydrogen in the lattice and at traps is given by thermodynamic equilibrium as first proposed by Oriani (1970). In the present study, it suffices to use a simplified approach by assuming the two limits of zero time for hydrogen diffusion in the conventional strain rate tests of Hagihara et al. (2008) and infinite time for hydrogen diffusion in the slow loading tests of Wang et al. (2005b, 2007).

1.1. Scope of study

First, the ability of various types of trap to bind hydrogen is assessed. The partitioning of hydrogen between the traps and the bulk lattice is analysed as a function of test time. Notched strength data are taken from the literature and used to establish a fracture criterion in the form of a locus of maximum principal tensile stress versus hydrogen concentration. To achieve this, an elastic-plastic FE analysis is performed on the notched geometries and the

stress distribution across the net section is determined. Finally, the data of Wang et al. (2007) for un-notched smooth specimens are compared with their results for notched specimens. We shall demonstrate that the fracture criterion as deduced from the notched tests is able to account for un-notched strength as a function of hydrogen concentration, provided due account is made for the stressed volume effect, as quantified by Weibull statistics.

2. A brief summary of the Oriani's theory

We begin our study by summarising the relative distribution of hydrogen in the lattice and at traps, in accordance with Oriani's theory. Hydrogen in a metal is either stored at normal interstitial lattice sites (NILS) or is trapped at microstructural defects such as dislocations, grain boundaries, interfaces and carbides. The concentration of hydrogen at NILS, also called the lattice hydrogen concentration, is given by

$$C_L = \theta_L \beta N_L, \tag{1}$$

where θ_L is the fraction of occupied interstitial lattice sites, β is the number of NILS per lattice atom and N_L is the number of lattice atoms per unit volume. Similarly, the concentration of hydrogen trapped at any given site is

$$C_T = \theta_T \alpha N_T \tag{2}$$

where θ_T is the fraction of occupied trapping sites, α is the number of atom sites per trap and N_T is the number of traps per unit volume. Oriani's equation states the equilibrium value of occupancy ratio of sites, in terms of

an equilibrium constant K, as

$$\frac{\theta_T}{1-\theta_T} = K\frac{\theta_L}{1-\theta_L}. \tag{3}$$

Since $\theta_L << 1$, this relation can be rephrased as

$$\theta_T \approx \frac{K\theta_L}{1+K\theta_L} = \frac{KC_L}{\beta N_L + KC_L}. \tag{4}$$

In turn, K is related to the the trap binding energy ΔH, the gas constant R and the absolute temperature T according to

$$K = \exp\left(\frac{-\Delta H}{RT}\right). \tag{5}$$

2.1. Implications of Oriani's equation

Upon making use of Eqs. (1), (3) and (5), contours of occupancy ratio of traps θ_T are plotted in Fig. 1 as a function of trap binding energy ΔH and lattice concentration C_L at $T = 298$ K. In order to do so, we assume that $\beta = 6$ and $N_L = 8.46\times10^{28}$ m^{-3} for BCC iron, following Sofronis and McMeeking (1989).

The value of θ_T is much more sensitive to ΔH than to C_L. Consequently, a logarithmic scale is used for C_L whereas a linear scale is used for ΔH. We note in passing the equivalence between C_L and θ_L via Eq. (1). It is clear from Fig. 1 that $\theta_T \approx 1$ for all values of C_L, (unless C_L is extremely small, less than 10^{-2} wppm) when ΔH is less than -50 kJ/mol. Such traps are generally termed "irreversible" and examples include carbides ($\Delta H = -72$ kJ/mol) and grain boundaries ($\Delta H = -48$ kJ/mol), see Novak et al. (2010). In contrast, traps for which $\Delta H \geq -20$ kJ/mol are empty of hydrogen, $\theta_T \approx 0$, (unless C_L has an exceptionally high value in excess of 10 wppm).

2.2. Dislocation traps

Now consider dislocation traps. The concentration of hydrogen $C_T^{(d)}$ trapped at dislocation cores is given by Eq. (2), with $\alpha = 1$, and θ_T given by Eqs. (3) and (5). However, the number of dislocation traps per unit volume $N_T^{(d)}$ increases with the von Mises plastic strain ε^p. Following Novak et al. (2010) we first relate $N_T^{(\mathrm{d})}$ to the dislocation density ρ_d and to the lattice parameter a of the crystal structure of host atoms according to

$$N_T^{(\mathrm{d})} = \sqrt{2}\rho_\mathrm{d}/a. \tag{6}$$

In turn, ρ_d scales with ε^p according to

$$\rho_\mathrm{d} = \begin{cases} \rho_0 + k\varepsilon^p & \varepsilon^p \leq 0.5 \\ 10^{16}\mathrm{m}^{-2} & \varepsilon^p > 0.5 \end{cases} \tag{7}$$

where $\rho_0 = 10^{10}$ m^{-2} is the dislocation density of the material at zero plastic strain and $k = 2 \times 10^{16}$ m^{-2}. The set of equations (1-7) gives the concentration of hydrogen $C_T^{(\mathrm{d})}$ that is trapped at dislocations. In order to specify the value of $C_T^{(\mathrm{d})}$, we need to know the values of (ε^p, C_L) and the binding energy for dislocation traps $\Delta H^{(\mathrm{d})}$. In general, ε^p is known as function of loading history and position. For example, it is known immediately for an uniaxial test-piece, and can be deduced from a elastic-plastic FE analysis for a notched specimen. The lattice concentration C_L is determined experimentally by thermal desorption spectroscopy (TDS) or by a related technique, along with a knowledge of the local hydrostatic stress σ_h, as discussed below. However, the value for $\Delta H^{(\mathrm{d})}$ is problematic as a wide range of values are quoted in the literature, ranging from $\Delta H^{(\mathrm{d})} = -15$ kJ/mol (Wang et al.,

2007) to $\Delta H^{(\mathrm{d})} = -60$ kJ/mol (Sofronis and McMeeking, 1989). We have already demonstrated that θ_T is sensitive to the value of ΔH when it lies within the range -50 kJ/mol to -10 kJ/mol, recall Fig. 1. In order to obtain an accurate estimate for the value of $\Delta H^{(\mathrm{d})}$, we proceed to analyse the hydrogen absorbability experiments of Yoshizawa and Yamakawa (1976).

2.3. Determination of the binding energy for dislocation traps from published data on hydrogen solubility

Yoshizawa and Yamakawa (1976) subjected un-notched bars of AISI 4135 steel to pre-selected levels of tensile strain, and then charged all specimens with hydrogen until equilibrium was established. Consequently, they held C_L fixed in all specimens while they varied the pre-strain prior to charging, and this led to different values of C_T from specimen to specimen. They measured $(C_L + C_T)$ as a function of ε^p by electrochemical permeation. This procedure was performed on specimens tempered at at $400°C$ (temper A) and on specimens tempered at $600°C$ (temper B). Their measurements of hydrogen concentration at $\varepsilon^p = 0$ show that $C_L = 576$ wppm for temper A, and $C_L = 196$ wppm for temper B. Using this, our analysis of their data proceeds as follows:

(i) We obtain θ_L from their measured C_L values via Eq. (1). To do so, we assume that $\beta = 6$ and $N_L = 8.46\times10^{28}$ m^{-3}, from Sofronis and McMeeking (1989).

(ii) Their measured value of $(C_L + C_T)$ are listed in Table 1 and Table 2, for temper A and temper B, respectively. We deduce immediately the values of C_T since C_L is known.

(iii) We use Eqs. (6–7) to calculate $N_T^{(\mathrm{d})}$ as a function of ε^p, assuming that the lattice parameter a equals 0.287 nm, which is representative of BCC iron, (Pearson, 1967).

(iv) $\theta_T^{(\mathrm{d})}$ is determined as a function of ε^p via Eq. (2), upon making the choice $\alpha = 1$.

(v) We finally solve for K in Eq. (3) and use it to calculate $\Delta H^{(d)}$ via Eq. (5).

Values for $\Delta H^{(\mathrm{d})}$ are included in Table 1 for temper A and in Table 2 for temper B, and are also plotted as a function of ε^p in Fig. 2. It is clear that $\Delta H^{(\mathrm{d})}$ is almost insensitive to the level of pre-strain and to the choice of tempering temperature. In the sequel, we shall adopt the mean value of $\Delta H^{(\mathrm{d})} = -37$ kJ/mol for AISI 4135 steel.

3. Method of analysis for the determination the hydrogen concentration

Commonly, the sensitivity of a steel to hydrogen embrittlement is determined by performing notched tensile tests on specimens that have been pre-charged with hydrogen, or are continuously charged during the test. In this section, we outline a simple procedure for determining the distribution of hydrogen in a pre-charged notched specimen under remote tension. Throughout our study we shall assume that the rate of pre-charging is sufficiently slow for the value of C_L to be spatially uniform after pre-charging and we denote this uniform value by $\langle C_L \rangle$. We shall consider the two asymptotic limits: (a) the test time much exceeds the diffusion time for hydrogen within the specimen, and (b) the test time is much less than the diffusion time. We

shall show below that the tests of Wang et al. (2005b) are at the limit where the test time much exceeds the the diffusion time for hydrogen within the specimen whereas the tests of Hagihara et al. (2008) lie at the limit of the the test time is much less than the diffusion time.

3.1. Slow tests in which hydrogen equilibrium is achieved

The pre-charged bar is subjected to axial tension at a sufficiently low rate that hydrogen equilibrium is maintained during the test. The chemical potential μ remains spatially uniform within the specimen. Remote from the stress-raising notch its magnitude is

$$\mu = \mu_0 + RT \ln C_L^{\infty} - \sigma_h^{\infty} V_H \tag{8}$$

where μ_0 is the chemical potential in the standard state, C_L^{∞} is the lattice hydrogen concentration remote from the notch and σ_h^{∞} is the hydrostatic stress remote from the notch. The partial molar volume of hydrogen in solid solution is denoted by V_H. In the vicinity of the notch root, the chemical potential is unchanged (as equilibrium is assumed), but the local hydrostatic stress σ_h modifies the lattice hydrogen concentration C_L according to

$$\mu = \mu_0 + RT \ln C_L - \sigma_h V_H. \tag{9}$$

Upon equating expressions (8) and (9) for the chemical potential, we obtain

$$C_L(\sigma_h) = C_L^{\infty} \exp\left(\frac{(\sigma_h - \sigma_h^{\infty})V_H}{RT}\right). \tag{10}$$

It remains to specify C_L^{∞}. Assuming that the stressed volume at the notch root is much smaller than the volume V of the specimen it follows that C_L^{∞} remains constant at the mean value attained after pre-charge $\langle C_L \rangle$. Therefore,

we can rewrite Eq. (10) as

$$C_L(\sigma_h) = \langle C_L \rangle \exp\left(\frac{(\sigma_h - \sigma_h^{\infty})V_H}{RT}\right), \tag{11}$$

to give the local hydrogen concentration in terms of the local hydrostatic stress σ_h. In Appendix A, a more rigorous description of hydrogen concentration development under an applied stress state is given where the approximation $C_L^{\infty} \approx \langle C_L \rangle$ is relaxed: this analysis demonstrates that Eq. (11) is accurate to better than 98% for the specimens analyzed here.

3.2. Rapid tests in which no lattice hydrogen diffusion can occur

In rapid tests, there is insufficient time for lattice hydrogen to diffuse, and consequently the total hydrogen concentration (lattice hydrogen concentration and trapped hydrogen concentration) is given by the initial hydrogen concentration, C^0, such that

$$C_L + C_T^{(d)} + C_T^{(gb)} + C_T^{(c)} = C^0. \tag{12}$$

where $C_T^{(d)}$, $C_T^{(gb)}$ and $C_T^{(c)}$ are the concentrations trapped at dislocations, grain boundaries and carbides, respectively. The partitioning between concentration at each trap and the lattice concentration C_L is in accordance with Oriani's theory, Eq. (3). This implicitly assumes that local rearrangement of hydrogen between lattice and traps occurs on a much shorter timescale than does long range diffusion. First, consider the hydrogen concentration at grain boundaries and carbide traps. The grain boundary trap density $N_T^{(gb)}$ and carbide trap density, $N_T^{(c)}$ remain constant during a rapid test. The large and negative values for the trap binding energy for grain boundaries ($\Delta H^{(gb)} = -48$ kJ/mol) and carbides ($\Delta H^{(c)} = -72$ kJ/mol) (Novak et al.,

2010), implies that the trap occupancy ratios are $\theta_T^{(gb)} \approx 1$ and $\theta_T^{(c)} \approx 1$, irrespective of the magnitude of C_L, recall Eq. (3) and Fig. 1. Consequently, the hydrogen concentration at saturated grain boundary traps $C_T^{(gb)}$ and carbide traps $C_T^{(c)}$ remain unchanged during the entire rapid test, so that we can rearrange Eq. (12) as

$$C_L + C_T^{(d)} = C^0 - C_T^{(gb)} - C_T^{(c)}. \tag{13}$$

All quantities on the right hand side of Eq. (13) remain constant during a rapid test. However, an increase in local plastic strain ε^p during a rapid test leads to an increase in the density $N_T^{(d)}$ of dislocation traps via Eq. (6) and Eq. (7) and hence to an increase in the concentration at dislocation traps $C_T^{(d)}$ via Eq. (2-5), using the parameters as detailed in sections 2.2 and 2.3 [1]. The value of C_L as a function of ε^p is then calculated from Eq. (13) to read

$$C_L(\varepsilon^p) + C_T(\varepsilon^p) = C_L(0) + C_T(0) = C^0 - C_T^{(gb)} - C_T^{(c)}. \tag{14}$$

For even modest values of ε^p, $N_T(\varepsilon^p) >> N_T(0)$ (see Eq. (7)) and hence $C_T(\varepsilon^p) >> C_T(0)$. We can then further simplify Eq. (14) to the form

$$C_L(\varepsilon^p) = C_L(0) - C_T(\varepsilon^p). \tag{15}$$

Recall that the relatively long charging times imply that $C_L(0)$ is spatially uniform after the pre-charge and its value is denoted by $\langle C_L \rangle$. Consequently, we can rewrite Eq. (15) as

$$C_L(\varepsilon^p) = \langle C_L \rangle - C_T(\varepsilon^p). \tag{16}$$

[1] $\alpha = 1$, $\Delta H = -37$ kJ/mol

4. Assessment of the notched strength of hydrogen-charged specimens

In order to analyse the significance of absorbed hydrogen in tensile tests on notched specimens we now turn our attention to the experimental failure strength data for notched tensile specimens from the literature. In section 4.1, the slow tests of Wang et al. (2005b) will be analysed; here, the test time much exceeds the diffusion time for hydrogen over a length scale of the net section radius. Then, in section 4.2, the rapid tests of Hagihara et al. (2008) will be analysed; here, the test time is much less than the diffusion time.

In both sets of reported experiments, round bars of diameter 10 mm were prepared from AISI 4135 steel, austenitized at 1133 K for one hour, quenched in oil and then tempered at 733 K for 1.5 hours. Specimens were notched circumferentially to a depth of 2 mm, and to three values of notch radius ρ =0.1, 0.25 and 0.8 mm, as detailed in Fig. 3. The elastic stress concentration factors are $K_t = 4.9$, $K_t = 3.3$ and $K_t = 2.1$, respectively.

In order to calculate the stress and strain state of the notched specimens at failure we use an axi-symmetric, elastic-plastic FE model, see Fig. 3. The FE mesh consists of 8880 bilinear quadrilateral elements, and the mesh density is increased in the vicinity of the notch in order to determine accurately the stress and strain state at the notch root. The FE analysis assumes of J_2 flow theory, with isotropic hardening. The hardening response is defined by the uniaxial tensile stress versus strain curve as measured by Wang et al. (2005b) on an un-notched specimen and absent any hydrogen; see Fig. 4. We note that Wang et al. (2005b) found that hydrogen charging did not change the shape of the stress-strain curve but only reduced the ductility. This jus-

tifies the use of the same tensile response given in Fig. 4 for both uncharged and charged specimens.

4.1. Slow tests in relation to the diffusion time

In this section we will analyse the set of slow tests on notched specimens, as performed by Wang et al. (2005b). Hydrogen was introduced into the samples by electrochemical charging at various current densities prior to testing. Charging and homogenization was carried out for 72 hours in order to achieve a spatially uniform lattice hydrogen concentration $C_L = \langle C_L \rangle$. The notched bar specimens were then loaded with a remote strain rate of $\dot{\varepsilon} = 8.3 \times 10^{-7}\mathrm{s}^{-1}$ in a tensile testing machine until the specimens failed. The hydrogen content of each specimen was detected by thermal desorption spectroscopy (TDS) immediately after failure. In their evaluation of the values for $\langle C_L \rangle$, Wang et al. (2005b) disregarded the high temperature peak of the TDS spectra, as they (correctly) argued that this peak is associated with irreversible hydrogen traps.

The net section tensile strength σ_{net} is defined as the maximum tensile load during the test divided by the initial, net cross-section area of the specimen. The dependence of σ_{net} on mean lattice concentration $\langle C_L \rangle$ is given in Fig. 5 from Wang et al. (2005b). It is clear from the figure that σ_{net} decreases with increasing hydrogen content, and σ_{net} decreases with decreasing notch root radius (and increasing K_t).

4.1.1. Assessment of hydrogen embrittlement: the role of hydrogen trapped at grain boundaries and carbides

We proceed to argue that hydrogen trapped at grain boundaries and at carbides plays a negligible role in degrading the tensile strength of the notched specimens, as reported in Fig. 5. The predicted θ_T for dislocation, grain boundary and carbide traps are plotted in Fig. 6 as a function of $\langle C_L \rangle$ upon making use of Eqs. (1-5). To do so we assume $\Delta H^{(d)} = -37$ kJ/mol for dislocations as obtained in Section 2.3 and make use of values $\Delta H^{(c)} = -72$ kJ/mol for carbides and $\Delta H^{(gb)} = -48$ kJ/mol for grain boundaries, as reported by Novak et al. (2010). For the range of values of $\langle C_L \rangle$ that were used by Wang et al. (2005b), the carbide and grain boundary traps are both fully saturated $\theta_T = 1$. This implies that these irreversible traps did not lead to the major drop in strength σ_{net} with increasing $\langle C_L \rangle$, as reported in Fig. 5. The lattice hydrogen and hydrogen trapped at dislocations remain as potential sources of hydrogen embrittlement. Consequently, in the remainder of this paper we will deal only with the dislocation traps and the reduced notation of C_T will be used to denote the trapped hydrogen concentration at dislocation traps.

4.1.2. Assessment of hydrogen embrittlement: the role of lattice hydrogen and hydrogen trapped at dislocations

Our overall goal is to generate a unique failure locus for local tensile stress σ_{22} versus local hydrogen concentration, that is able to rationalise all the data shown in Fig. 5. But there is a choice in the nature of hydrogen concentration that might be dictating the strength. Specifically, there is a choice in constructing a failure locus such that σ_{22} is expressed in terms

of lattice concentration C_L or concentration at dislocation traps C_T. The local lattice concentration C_L depends upon the local hydrostatic stress in accordance with Eq. (11), and the concentration of hydrogen at dislocation traps C_T follows via Eqs. (2-7).

Our strategy can be simply stated as follows. At the observed failure strength σ_{net} for any notched specimen, and pre-charged to a selected value of $\langle C_L \rangle$, the local stress distribution $\sigma_{22}(x_1)$ along the net section is determined by elasto-plastic FE analysis. Likewise, the hydrostatic stress distribution $\sigma_h(x_1)$ is calculated and thereby $C_L(x_1)$ using, Eq. (11). The distribution $C_T(x_1)$ then follows from Eq. (2-7), by making use of the known distribution of $\varepsilon^p(x_1)$ from the FE analysis. In order to help explain the above procedure we give salient examples of the FE results.

Stress-strain distribution ahead of notch.

We plot the maximum tensile principal stress σ_{22} and the von Mises plastic strain ε^p distributions as a function of distance x_1 ahead of the notch root, on the mid-plane, $x_2 = 0$, at failure. Results are shown for selected states of hydrogen pre-charge and a notch radius of $\rho = 0.1$ mm The profiles labeled (A,B,C,D) in Fig. 7 corresponds to the data points labeled with the same letters in Fig. 5. Specimen A contained no hydrogen and failed by micro-void coalescence. In contrast, the remaining specimen contained hydrogen and failed by cleavage. We thus expect such brittle fracture to initiate at the location of peak σ_{22} in the charged specimens.

As the level of hydrogen is increased from zero (specimen A) to a high value (specimen D), σ_{net} drops and the size of the plastic zone at the notch root decreases sharply. Note that the plastic zone is almost non-existent for

specimen D and hence this specimen is not included in Fig. 7b. The peak value of σ_{22} is attained at an intermediate location between the notch root and the plastic zone boundary, see Fig. 7a. In contrast, ε^p is a maximum at the notch root, see Fig. 7b.

We proceeded to argue that the hydrogen concentration has attained the equilibrium distribution at failure. Recall that the distance from the notch root to the site of maximum stress ahead of the notch root is on the order of 0.2 mm. For equilibrium to be achieved, the diffusion distance of hydrogen l must exceed this distance. Now invoke the random walk equation $l = \sqrt{Dt_f}$ where $D = 3.8 \times 10^{-11}\text{m}^2/\text{s}$ (Wang et al., 2005b) and t_f is the test time. The diffusion length l is on the order of 0.2-0.3 mm, and listed in Table 3 for specimen B to D (specimen A contained no hydrogen). Since l is comparable to the required diffusion distance of 0.2 mm, we conclude that equilibrium of hydrogen concentration has been established. Additional support for this view is obtained upon noting that Wang et al. (2005a) performed additional notched tests at an applied displacement rate which was reduced by a factor of 50 and observed no change in measured strength.

Calculation of C_L and C_T distributions.

We proceed to calculate the $C_L(\sigma_h)$ and C_T distributions, as a function of x_1, as follows. Since the diffusion time is less than the test time in the slow tests of Wang et al. (2005b), $C_L(\sigma_h)$ can be calculated directly from Eq. (11) and C_T is obtained from Oriani's theory using Eqs. (2-7).

In order to assess the roles of C_L and C_T upon the embrittlement phenomena we attempt to construct a unique failure locus of σ_{22} versus C_L from the measured data. In similar manner we shall assess whether the data of

Wang et al. (2005b) suggests a unique failure locus of σ_{22} versus C_T. Consider a particular fracture test, for example the test with $\rho = 0.1$ mm and $\langle C_L \rangle = 2.20$ wppm, i.e. case D as defined above. Recall that $C_L(x_1)$ is calculated from the known distribution of $\sigma_h(x_1)$ and $\langle C_L \rangle$ using Eq. (10). Then re-plot $\sigma_{22}(x_1)$ and $C_L(x_1)$ as $\sigma_{22}(C_L)$ by treating x_1 as an intrinsic variable, see Fig. 8a. This procedure is repeated for other values of $\langle C_L \rangle$. Each trajectory gives the local maximum principal stress σ_{22} ahead of the notch and the hydrogen concentration at this point.

A unique failure locus can be constructed in σ_{22} versus $C_L(\sigma_h)$ space by drawing the outer envelope to the individual trajectories, as done in Fig. 8a. We note that this failure envelope is the locii of peak values σ_f of the σ_{22} versus $C_L(\sigma_h)$ curves. A similar construction has been attempted for $\rho = 0.1$ mm notched tests by plotting σ_{22} versus C_T for each sample at failure, see Fig. 8b. The distribution $C_T(x_1)$ for any given value of $\langle C_L \rangle$ is obtained from Eq. (2-7), and upon treating x_1 as an intrinsic variable we obtain σ_{22} versus C_T. Now, however, the relative locations of the trajectories is such that an outer failure envelope cannot be constructed in σ_{22} versus C_T space. We conclude that the notched data for $\rho = 0.1$ mm can only be rationalised in terms of of a unique failure locus in σ_f versus C_L space, recall Fig. 8a.

It remains to explore whether the same failure locus is generated from the data of σ_{net} versus $\langle C_L \rangle$ for $\rho = 0.25$ mm and $\rho = 0.8$ mm. Upon repeating the above procedure, the deduced failure loci for the 3 values of ρ are compared in Fig. 9. It is clear that they collapse onto a single master curve, in support of this simple failure criterion. The degree of scatter is portrayed by giving an upper and lower limit for the failure locus.

An additional assessment of this approach is to explore whether the same failure locus applies to test data on AISI 4135 steel, but now for rapid tests in relation to the diffusion time. This assessment is performed in the following section.

4.2. Rapid tests in relation to the diffusion time

Hagihara et al. (2008) performed identical tests on AISI 4135 steel to those of Wang et al. (2005b), but at high remote strain rate of $\dot{\varepsilon} = 1.7 \times 10^{-4}\text{s}^{-1}$. Consequently, test time t_f is now in the range 7-23 s, and the corresponding diffusion length $\sqrt{Dt_f}$ is in the range $16 - 29$ μm (upon assuming $D = 3.8 \times 10^{-11}\text{m}^2/\text{s}$ as given by Wang et al. (2005b)). This diffusion distance is 1-2 orders of magnitude less than the plastic zone size at the notch root at failure. Thus, we can assume negligible diffusion occurs during the tests and the tests can be considered as rapid in relation to the diffusion time. The details of the rapid notch tests are the same as those performed by Wang et al. (2005b) and are summarised follows. Hagihara et al. (2008) performed so-called conventional strain rate tensile tests on V-notched specimens with varying notch radii and at different hydrogen charging conditions. The specimen geometries were identical to the ones discussed in section 4.1 and are shown in Fig. 3. Hydrogen was introduced into the samples by electrochemical charging at various current densities. Charging and homogenization was carried out for 72 hours so that a spatially uniform lattice hydrogen concentration was attained before the uniaxial tension test starts.

The results of the notch tests are plotted as σ_{net} versus $\langle C_L \rangle$ in Fig. 10. In broad terms, the trends are the same as in Fig. 5. The FE analysis, as reported above, is again used to obtain the $\sigma_{22}(x_1)$ and $\varepsilon^p(x_1)$ distribution

directly ahead of the notch for selected values ρ and σ_{net}. We make use of Eq. (16) to determine $C_L(x_1)$ and, upon using x_1 as an intrinsic variable, we re-plot σ_{22} as a function of C_L for each test. The results of this procedure are given in Fig. 11a for the choice $\rho = 0.8$ mm. The upper and lower limits of scatter in σ_f versus C_L are transcribed from Fig. 9 to Fig. 11: the failure envelope for the rapid tests is in good agreement with that for the slow tests.

The overall failure envelope in terms of upper and lower limits of scatter is plotted as σ_f versus C_L for the rapid tests, with $\rho = 0.1$ mm, 0.25 mm and 0.8 mm, see Fig .11b. The figure includes the failure envelope from Fig. 9 for the slow tests of Wang et al. (2005b). Excellent agreement is noted. We conclude that a unique failure locus exists for all tests, and can be treated as a material property.

5. Assessment of un-notched strength of hydrogen-charged specimens

The above failure locus is able to correlate a diverse range of notched tests. It remains to be shown that the same failure locus can rationalise the un-notched strength in the presence of hydrogen. Such an assessment is given in the current section by analysis of the comprehensive test results of Wang et al. (2007) for AISI 4135 steel for both notched and un-notched specimens. The stress-strain curve for a hydrogen-free un-notched bar of this material is reported in Fig. 4: the steel is slightly stronger than that is reported in the Wang et al. (2005b) study due to a lower tempering temperature. The notched specimen geometry, charging conditions and stain rate employed by Wang et al. (2007) were identical to those used in Wang et al.

(2005b). Thus, these tests were again slow in relation to the diffusion time. Un-notched bars of diameter $d = 5$ mm and gauge length $l = 100$ mm were also tested at various hydrogen charging conditions.

The findings of Wang et al. (2007) are summarised in Fig. 12. In Fig. 12a the net section strength σ_{net} is given as a function of $\langle C_L \rangle$ for specimens with notch radii of $\rho = 0.1$ mm, $\rho = 0.8$ mm and also for un-notched specimens. The strength data for the notched specimen are in good agreement with those of Wang et al. (2005b), compare Fig. 12a with Fig. 5. Wang et al. (2007) attempted to correlate their strength data for both notched and un-notched tests by assuming that failure occurs when the maximum value of σ_{22} in the specimen attains a critical value σ_f which depends upon the lattice hydrogen concentration C_L. They corrected C_L for the effect of hydrostatic stress via Eq. (10). They did not plot the trajectory of σ_f versus C_L for each specimen, as done here in Fig. 8a, but they did postulate a critical failure locus of σ_{22} versus $C_L(\sigma_h)$, and used an elastic-plastic FE analysis in order to calculate $\sigma_h(x_1)$ and $\sigma_{22}(x_1)$. Their predictions of σ_f versus $C_L(\sigma_h)$ are repeated here in Fig. 12b. We note that their failure locii for $\rho = 0.1$ mm and $\rho = 0.8$ mm overlap, however the failure locus for their un-notched tests lies significantly below the locii for notched tests. We have performed an independent FE analysis of their notched specimens at failure by making use of the uniaxial stress versus strain response of the steel (in the absence of hydrogen) as measured by Wang et al. (2007) and included in Fig. 4. Specifically, we determined the trajectory of σ_{22} versus $C_L(\sigma_h)$ for each of their specimens and thereby generated an outer envelope to define the failure locus. Our predictions are in close agreement with their plots

of Fig. 12b and consequently there is no need to show them. It remains to rationalise the low strength of the un-notched specimens in relation to their notched counterparts.

5.1. Application of Weibull Statistics

It remains to explore possible reasons for the weaker response of the un-notched specimens compared to the notched ones, recall Fig. 12b. Recall that hydrogen induces brittle inter-granular failure, in a manner which is reminiscent of the failure of a polycrystalline ceramic. For such brittle solids, failure initiates from the largest inherent flaw, and probability of large flaws increases with the size of stressed volume. Weakest link theories of strength, such as Weibull theory, attempt to account for such size effects. Here, we proceed to make use of Weibull statistics in an attempt to bring into alignment the notched and un-notched strength strength data of Wang et al. (2007).

5.2. Use of Weibull theory

Recall that the probability of survival P_s for a stressed component of volume V can be estimated from the distribution of maximum tensile principal stress $\sigma_{max}(x_i)$ throughout the body, according to the Weibull relation

$$P_s(\sigma_{ij}, V) = \exp\left\{ -\int_V \left(\frac{\sigma_{max}}{\sigma_0}\right)^m \frac{dV}{V_0} \right\}. \tag{17}$$

Here, the Weibull modulus m gives the variability of strength whereas σ_0 is a measure of average strength for a volume V equal to a reference volume V_0. Here, we take V_0 to be equal to the volume of the un-notched specimens of Wang et al. (2007) and so, for the un-notched specimen, the Weibull relation Eq. (17) reduces to

$$P_s(\sigma_0) = \exp\left\{ -\left(\frac{\sigma}{\sigma_0}\right)^m \right\}. \tag{18}$$

We emphasize that Eq. (18) gives the distribution in strength for a large population of nominally identical tensile specimens, subjected to the same level of hydrogen pre-charge. Unfortunately, hydrogen tests are sophisticated and expensive and repeat tests are rarely performed. Consequently, it is not possible to measure m values directly from an observed distribution in strength from multiple specimens. Here, we adopt the following pragmatic approach:

(i) we assume a value for m, say $m = 30$.

(ii) We deduce the value of σ_0 from the un-notched specimen tests using Eq. (18) and assuming (arbitrarily) $P_s = 0.1$. Note that the deduced value of σ_0 is sensitive to $\langle C_L \rangle$. The calculated values for σ_0 are shown in Fig. 13a for a choice of $m = 30$.

(iii) We evaluate Eq. (17) numerically from the FE solution for the notched tests, by making use of the FE solution for $\sigma_{max}(x_i)$ throughout the volume of the specimen, for a selected value of σ_{net} at failure. The procedure is repeated using various trial values of σ_{net} until the result $P_s = 0.1$ is obtained.

But there remains a subtlety in procedure since σ_0 is a function of C_L (recall Fig. 13a) and two methods are used to account for this.

Method A

We assume that σ_0 in the notched tests is spatially uniform and is given by the mean concentration of the lattice hydrogen $\langle C_L \rangle$, in accordance with the calibration curve of Fig. 13a.

Method B

We take into account the fact that C_L varies in the vicinity of the notch, due to the variation of σ_h with position, recall Eq. (10). If we employ the calibration curve of Fig. 13a at each material point then σ_0 will vary with position. The Weibull integral Eq. (17) is now evaluated for a distribution of both $\sigma_{max}(x_i)$ and $\sigma_0(x_i)$.

The results of both methods are compared in Fig. 13b for the choice of $m = 30$. The predictions are given in the form of σ_{net} at failure versus $\langle C_L \rangle$ for the notched tests, and are compared against the measured values of Wang et al. (2007). We emphasize that we take the un-notched data as the calibration curve for σ_0 as a function of $\langle C_L \rangle$ and thus we do not make a prediction of the un-notched strengths.

Upon choosing $m = 30$ good agreement is noted for σ_{net} at failure versus $\langle C_L \rangle$ for both values of ρ, and there is only a small sensitivity of the predictions to the choice of method A or B. Additional simulations were performed for other values of m, and it was found that agreement was reasonable for m in the range of 25 to 35.

6. Concluding Remarks

Our study has considered possible sources of hydrogen embrittlement in a high strength steel AISI 4135 as reported by Wang et al. (2005b), Wang et al. (2007) and Hagihara et al. (2008). A failure locus in terms of maximum principal tensile stress versus C_L is able to rationalise the un-notched and notched strength in both slow and fast tests relative to the diffusion time for hydrogen. Our study has also revealed the relative potency of various traps in AISI

4135 steel. The trap binding energy of dislocation traps is estimated to be $\Delta H^{(d)} = -37$ kJ/mol. This renders dislocation traps as relatively reversible compared to grain boundary and carbide traps. Hydrogen that is trapped at irreversible trapping sites (grain boundaries and carbides) are found to be always fully saturated for the range of hydrogen charging conditions employed in the experiments of Wang et al. (2005b, 2007) and Hagihara et al. (2008). Therefore hydrogen trapped at these irreversible sites cannot be responsible for the observed decrease in strength of AISI 4135 steel. Moreover, the fracture strength did not correlate with the concentration of hydrogen trapped at dislocation cores.

The data of Wang et al. (2007) shows that un-notched bars pre-charged with hydrogen are anomalously weak compared to their notched counterparts. This discrepancy can be explained by considering the stressed volume effect using weakest link Weibull statistics. This has immediate implications in the engineering design of large structural components that are exposed to hydrogen. A topic for future study is the extrapolation of laboratory test data to such structures, and whether such size effects are indeed present at large scales.

Table 1: Extraction of dislocation binding energy for the AISI 4135 steel tempered at 400 C° (temper A) using the solubility data from Yoshizawa and Yamakawa (1976).

ε^p	$C_L + C_T$ (wppm)	C_L (wppm)	$C_T^{(\mathrm{d})}$ (wppm)	$\Delta H^{(d)}$ (kJ/mol)
1.95×10^{-4}	576	576	0	-
3.31×10^{-3}	699	576	123	-33.6
5.05×10^{-3}	835	576	259	-36.2
1.19×10^{-2}	1030	576	454	-33.7
1.95×10^{-2}	1710	576	1134	-38.2
2.40×10^{-2}	2030	576	1454	-39.4
4.01×10^{-2}	2840	576	2264	-37.6

Table 2: Extraction of dislocation binding energy for the AISI 4135 steel tempered at 600 C° (temper B) using the solubility data from Yoshizawa and Yamakawa (1976).

ε^p	$C_L + C_T$ (wppm)	C_L (wppm)	$C_T^{(d)}$ (wppm)	$\Delta H^{(d)}$ (kJ/mol)
2.15×10^{-4}	196	196	0	-
7.45×10^{-3}	318	196	122	-32.9
1.63×10^{-2}	921	196	725	-37.5
2.40×10^{-2}	1670	196	1474	-42.6

Table 3: Mean diffusion distance $l = \sqrt{Dt_f}$ of hydrogen during the tension test for the cases labeled with B, C and D in Fig. 5.

specimen label	t_f	l
B	2.89×10^3 s	331 μm
C	1.57×10^3 s	244 μm
D	8.43×10^2 s	179 μm

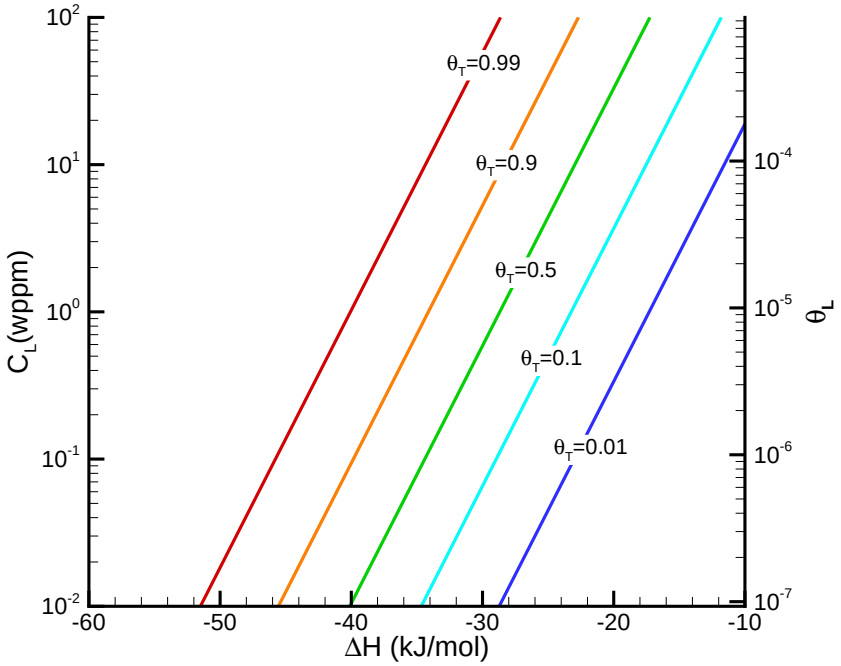

Figure 1: The effect of lattice hydrogen concentration C_L and trap binding energy ΔH on the trap occupancy ratio θ_T.

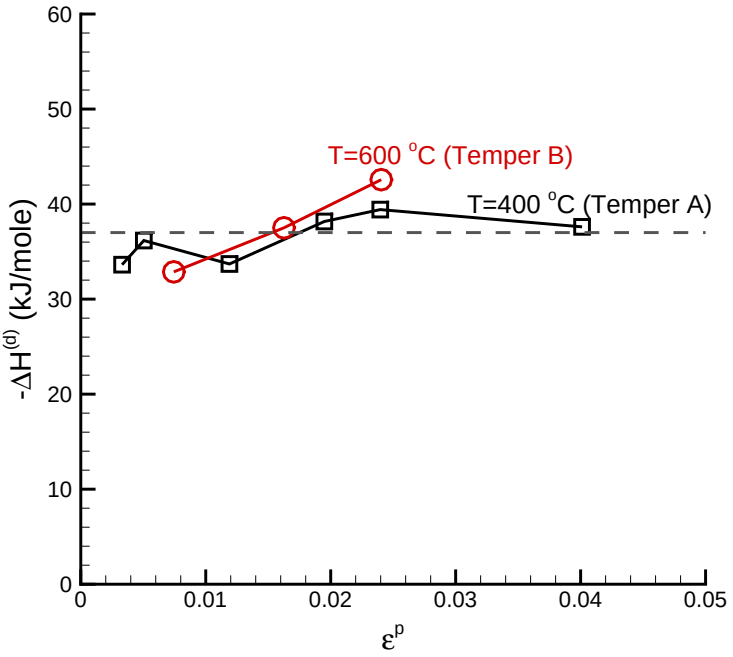

Figure 2: The dislocation trap binding energy $\Delta H^{(d)}$ for AISI 4135 steel tempered at 400° (temper A) and tempered at 600° (temper B) extracted from the experimental data of Yoshizawa and Yamakawa (1976).

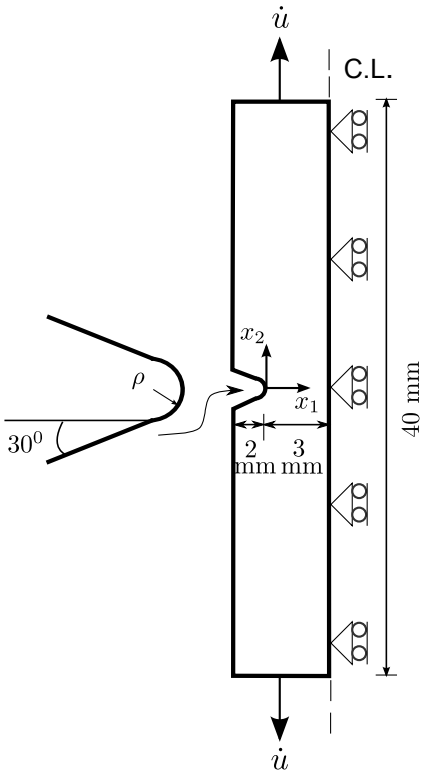

Figure 3: Sketch of the notched tensile bars used in Wang et al. (2005b), Wang et al. (2007) and Hagihara et al. (2008). The boundary conditions applied to the axi-symmetric specimen in the FE analysis are also indicated.

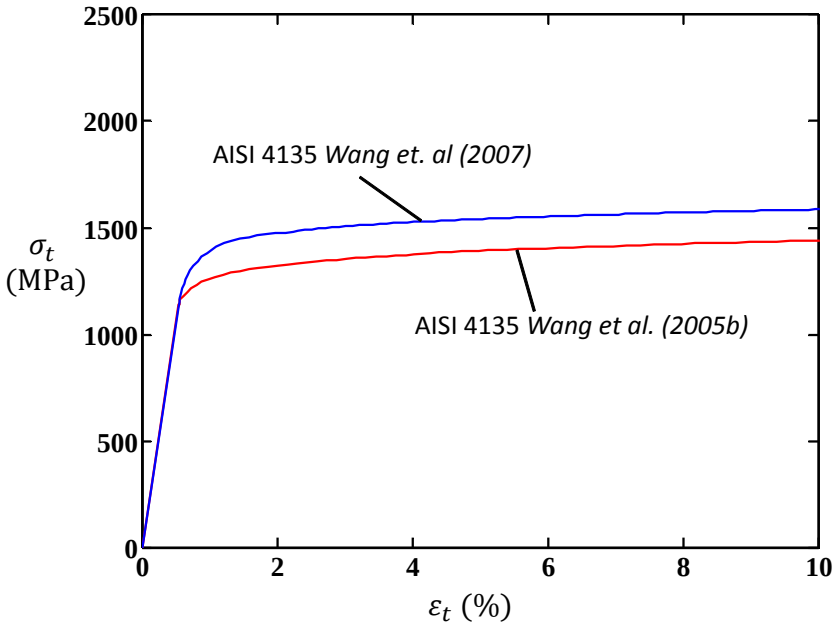

Figure 4: The uniaxial tensile stress versus strain curves for AISI 4135 steel as measured by Wang et al. (2005b) and Wang et al. (2007). This data was used as the material model in FE calculations.

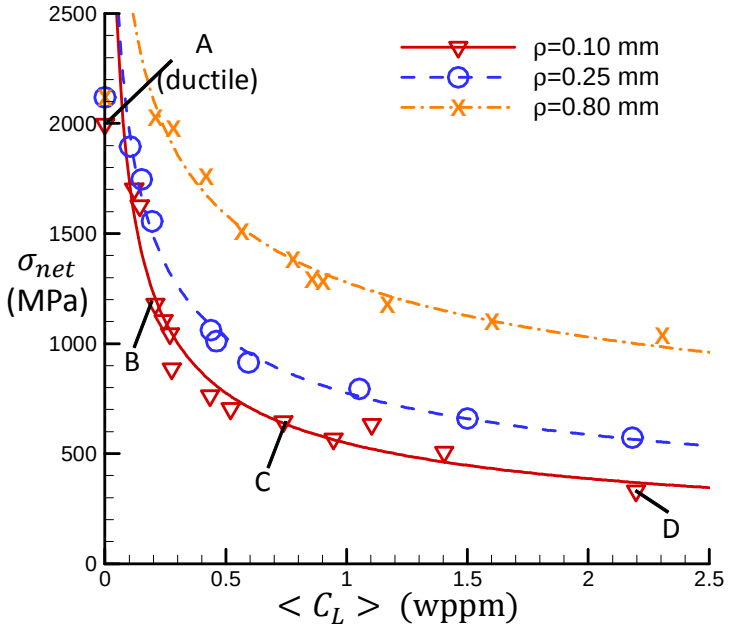

Figure 5: Net section strength of notched specimens as a function of the lattice hydrogen concentration $\langle C_L \rangle$ after pre-charging as measured in slow loading tests by Wang et al. (2005b). Data is shown for three values of the notch root radius ρ.

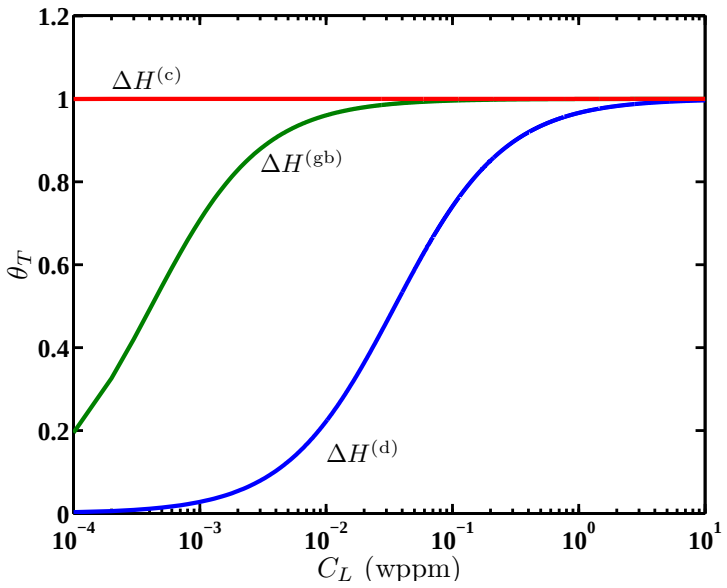

Figure 6: Trap occupancy ratio of hydrogen at carbide, grain-boundary and dislocation traps as a function of lattice hydrogen concentration C_L.

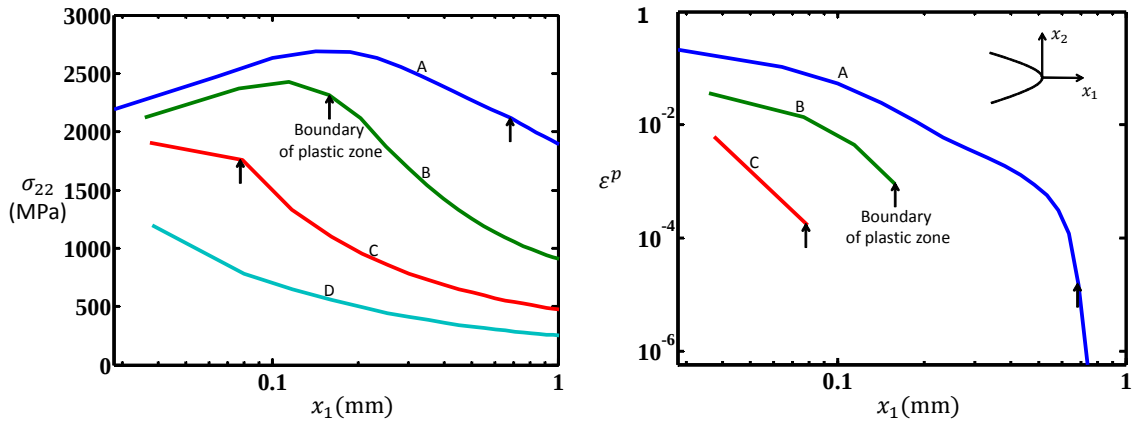

Figure 7: FE predictions of the distribution of (a) the stress σ_{22} and (b) von Mises plastic strain ε^p along the net-section ($x_2 = 0$) at failure in the $\rho = 0.1$ mm specimens of Wang et al. (2005b). The predictions are shown for selected specimens labeled A through D in Fig. 5.

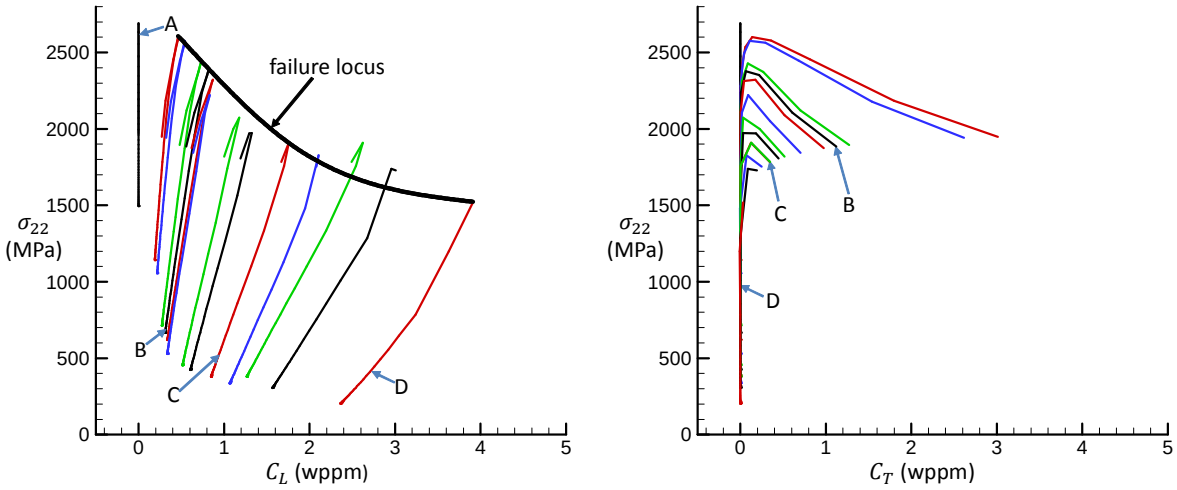

(a) (b)

Figure 8: Predictions of trajectories of the local tensile stress σ_{22} versus (a) lattice hydrogen concentration C_L and (b) concentration of hydrogen trapped at the dislocations C_T in the $\rho = 0.1$ mm notched specimens of Wang et al. (2005b). The trajectories are calculated assuming slow loading in relation to the diffusion time and selected trajectories A-D are labeled from Fig. 5.

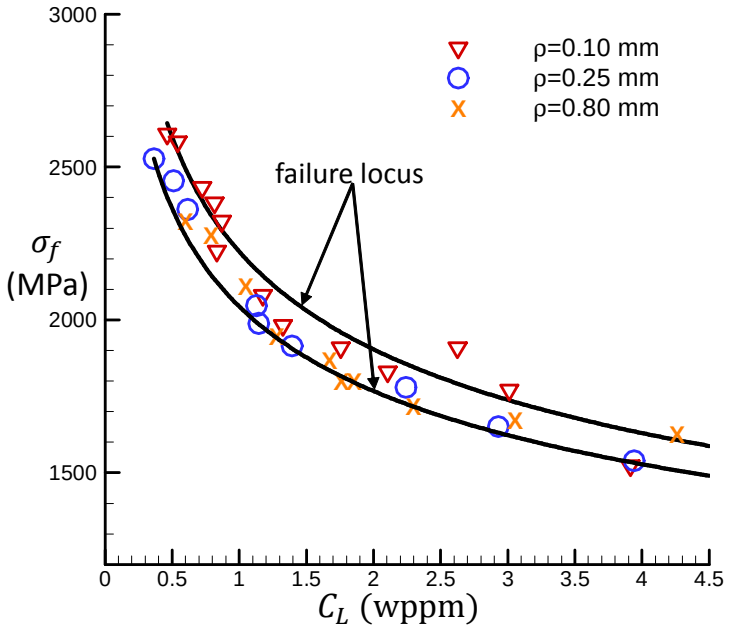

Figure 9: Predictions of the failure locus for the data of Wang et al. (2005b) for three different values of the notch root radius ρ. An upper and lower limit for the failure locus is sketched to reflect the degree of scatter in the data.

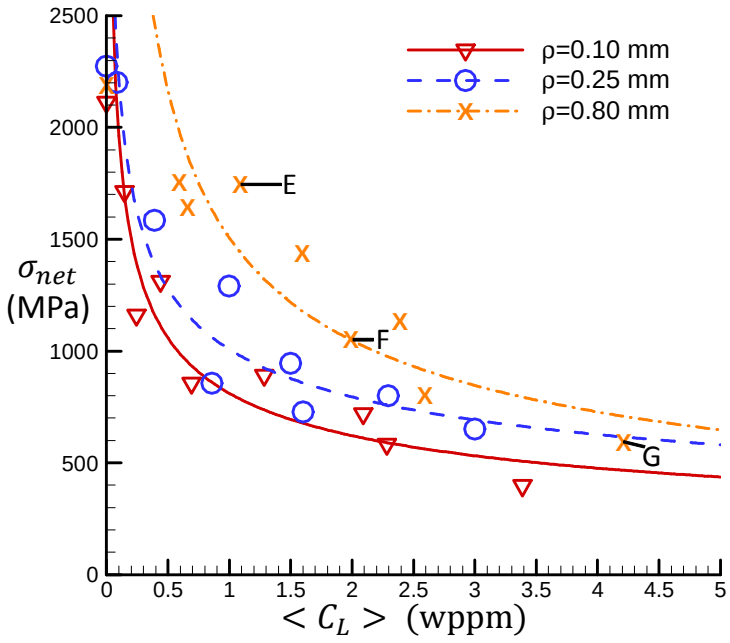

Figure 10: Net section strength of notched specimens as a function of the mean lattice hydrogen concentration $\langle C_L \rangle$ after pre-charging as measured in fast loading tests by Hagihara et al. (2008). Data is shown for three values of the notch root radius ρ.

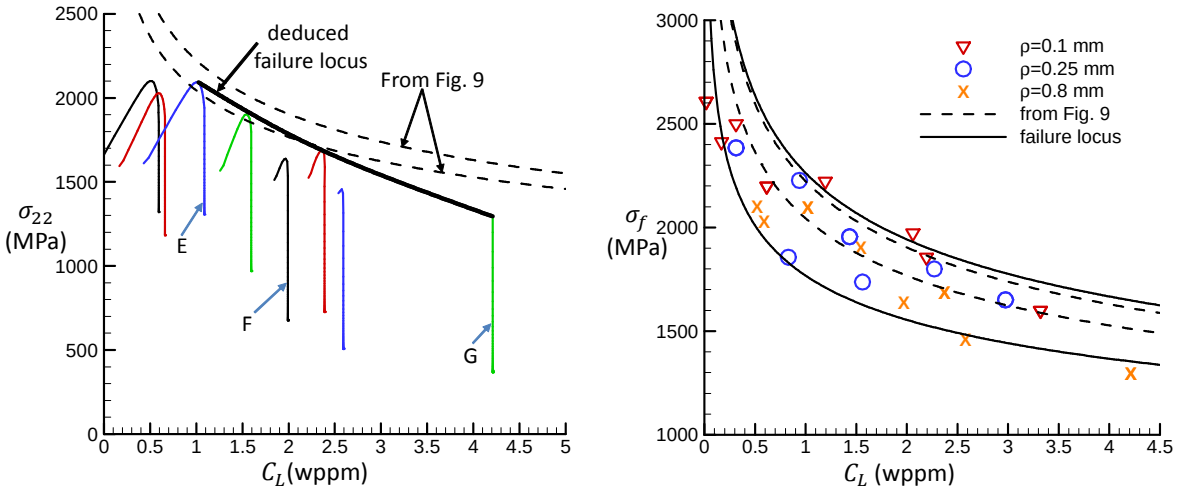

Figure 11: (a) Predictions of trajectories of the local tensile stress σ_{22} versus lattice hydrogen concentration C_L for the $\rho = 0.8$mm notched specimen of Hagihara et al. (2008). The failure locus based on these trajectories is also sketched. (b) Predictions of the failure loci from the for the data of Hagihara et al. (2008) for three different values of the notch root radius ρ. The predictions of the loci are seen to overlap. In (a) and (b) scatter bands from Fig. 9 of the failure loci extracted from the Wang et al. (2005b) data are also included.

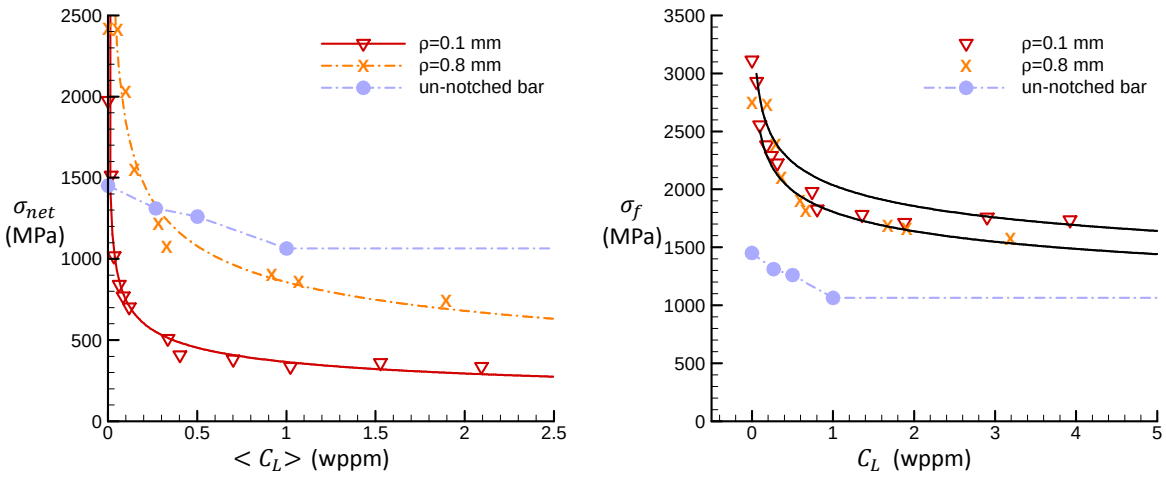

Figure 12: (a) Net section strength of notched specimens as a function of the mean lattice hydrogen concentration $\langle C_L \rangle$ after pre-charging as measured in slow loading tests by Wang et al. (2007). Data is shown for two values of the notch root radius ρ and a un-notched specimen. (b) Predictions of the failure strength σ_f as a function of the local lattice hydrogen concentration at that location for the tests of Wang et al. (2007).

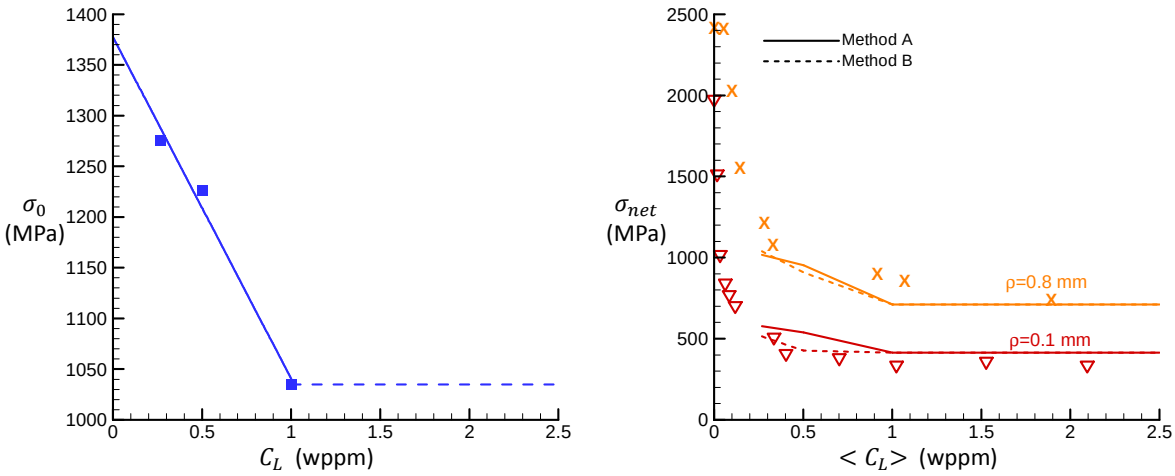

(a) (b)

Figure 13: (a) Predictions of the dependence of the reference stress σ_0 as a function of the lattice hydrogen concentration C_L from the un-notched bar tests of Wang et al. (2007). (b) Predictions of the net section failure stress σ_{net} as a function of mean hydrogen concentration $\langle C_L \rangle$ after pre-charging in the tests of Wang et al. (2007). The predictions using Weibull statistics with $m = 30$ and two analysis methods are included.

Appendix A. Exact calculation of the lattice hydrogen distribution in slow loading tests

Consider a pre-charged specimen of volume V with a uniform distribution of lattice hydrogen of magnitude $\langle C_L \rangle$. When the specimen is subjected to a non-uniform stress state (as in the case of the uniaxial tension of the notched specimen) the hydrogen re-distributes itself in the specimen due to the combined effects of hydrostatic stress and plastic strain. Mass conservation of the hydrogen dictates that at any stage of deformation we have

$$\langle C_L \rangle V = \int_V C_L dV + \int_V C_T dV, \tag{A.1}$$

where $C_L(x_i)$ and $C_T(x_i)$ are the local concentrations of lattice hydrogen and hydrogen trapped in the dislocation cores, respectively. If the rate of loading is sufficiently slow that the hydrogen diffusion times are small compared to the loading times, then the hydrogen remains in a state of equilibrium such that its chemical potential

$$\mu = \mu_0 + RT \ln C_L - \sigma_h V_H, \tag{A.2}$$

is spatially invariant. The lattice hydrogen concentration is then given in terms of the known spatial distribution of the hydrostatic stress $\sigma_h(x_i)$ as

$$C_L = C_L^0 \exp\left(\frac{\sigma_h V_H}{RT}\right), \tag{A.3}$$

in terms of the spatially invariant reference concentration

$$C_L^0 \equiv \exp\left(\frac{\mu - \mu_0}{RT}\right). \tag{A.4}$$

Combining Eqs. (A.1) , (A.3) and Eqs. (1-3) gives

$$\langle C_L \rangle V = C_L^0 \int_V \exp\left(\frac{\sigma_h V_H}{RT}\right) dV + \int_V \frac{K C_L^0 \exp(\frac{\sigma_h}{RT})}{\beta N_L - C_L^0 \exp(\frac{\sigma_h}{RT}) + K C_L^0 \exp(\frac{\sigma_h}{RT})} N_T dV, \tag{A.5}$$

which can be solved to obtain C_L^0. The distribution $C_L(x_i)$ follows from Eq. (A.3). Direct comparison have been made between the precise formula Eq. (A.5) for the un-notched and notched specimens, as tested by Wang et al. (2005b, 2007). The agreement is within a few percent in all cases.

Acknowledgements

The authors wish to acknowledge the Mitsubishi Heavy Metal Industries for the financial support.

References

Birnbaum, H., Sofronis, P., 1994. Hydrogen-enhanced localized plasticity a mechanism for hydrogen-related fracture. Materials Science and Engineering: A 176 (1-2), 191 – 202.

Gangloff, R., 2003. 6.02 - hydrogen-assisted cracking. In: in Chief: A A I. Milne, E., Ritchie, R. O., , Karihaloo, B. (Eds.), Comprehensive Structural Integrity. Pergamon, Oxford, pp. 31 – 101.

Gerberich, W. W., Oriani, R. A., Lii, M. J., Chen, X., Foecke, T., 1991. The necessity of both plasticity and brittleness in the fracture thresholds of iron. Phil. Mag. A 63, 363–376.

Hagihara, Y., Ito, C., Hisamori, N., Suzuki, H., Takai, K., Akiyama, E., 2008. Evaluation of delayed fracture characteristics of high strength steel based on csrt method. Tetsu To Hagane-Journal of the Iron and Steel Institute of Japan 94 (6), 215–221.

Jiang, D., Carter, E. A., 2004. First principles assessment of ideal fracture energies of materials with mobile impurities: implications for hydrogen embrittlement of metals. Acta Materialia 52 (16), 4801 – 4807.

Li, D., Gangloff, R., Scully, J., 2004. Hydrogen trap states in ultrahigh-strength aermet 100 steel. Metallurgical and Materials Transactions A 35, 849–864.

Novak, P., Yuan, R., Somerday, B., Sofronis, P., Ritchie, R., 2010. A statistical, physical-based, micro-mechanical model of hydrogen-induced inter-

granular fracture in steel. Journal of the Mechanics and Physics of Solids 58 (2), 206 – 226.

Oriani, R., 1970. The diffusion and trapping of hydrogen in steel. Acta Metallurgica 18 (1), 147 – 157.

Oriani, R. A., 1972. Mechanistic Theory of Hydrogen Embritlement of Steels. Berichte Der Bunsen-Gesellschaft Fur Physikalische Chemie 76 (8), 848–857.

Pearson, W., 1967. A Handbook of Lattice Spacings And Structures Of Metals And Alloys. Pergamon.

Serebrinsky, S., Carter, E., Ortiz, M., 2004. A quantum-mechanically informed continuum model of hydrogen embrittlement. Journal of the Mechanics and Physics of Solids 52 (10), 2403 – 2430.

Sofronis, P., McMeeking, R., 1989. Numerical analysis of hydrogen transport near a blunting crack tip. Journal of the Mechanics and Physics of Solids 37 (3), 317 – 350.

Thomas, R., Scully, J., Gangloff, R., 2003. Internal hydrogen embrittlement of ultrahigh-strength aermet 100 steel. Metallurgical and Materials Transactions A 34, 327–344.

Troiano, A. R., 1960. The role of hydrogen and other interstitials in the mechanical behaviour of metals. Trans. ASM. 52, 54–80.

Wang, M., Akiyama, E., Tsuzaki, K., 2005a. Crosshead speed dependence

of the notch tensile strength of a high strength steel in the presence of hydrogen. Scripta Materialia 53 (6), 713 – 718.

Wang, M., Akiyama, E., Tsuzaki, K., 2005b. Effect of hydrogen and stress concentration on the notch tensile strength of aisi 4135 steel. Materials Science and Engineering A 398 (1-2), 37 – 46.

Wang, M., Akiyama, E., Tsuzaki, K., 2007. Effect of hydrogen on the fracture behavior of high strength steel during slow strain rate test. Corrosion Science 49 (11), 4081 – 4097.

Yamasaki, S., Bhadeshia, H., 2006. M4c3 precipitation in fe-c-mo-v steels and relationship to hydrogen trapping. Proceedings of the Royal Society A: Mathematical, Physical and Engineering Science 462 (2072), 2315–2330.

Yoshizawa, S., Yamakawa, K., 1976. The role of hydrogen absorbability in hydrogen embrittlement of high strength steel.